Electronic Journal of Structural Engineering

Original Article

Cite this: DOI:10.56748/ejse.24757

Received Date: 21 January 2024
Accepted Date: 20 August 2025

1443-9255
https://ejsei.com/ejse

Determination of Effective Stiffness Characteristics of Unreinforced Masonry Using Numerical Homogenization

Shakarneh Omar M. D.

Novosibirsk State University of Architecture and Civil Engineering (Sibstrin), Russia.
Corresponding author: oshakarneh@gmail.com

Abstract

The article presents a homogenization method for determining the effective properties of brickwork through numerical modeling. The selection of representative volume elements (RVEs) for characterizing masonry is justified. Numerical experiments demonstrate that reliable stress-strain data require testing a fragment of nine brick rows (four bricks wide). A nine-row stretcher-bond fragment serves as a representative component for multi-row brickwork of any configuration, enabling deformation analysis without large-scale experiments. A method is proposed to determine the stiff characteristics of unreinforced masonry as an anisotropic homogeneous body using numerical loading simulations. The stiffness coefficient matrix is derived from finite element analysis (FEA) under compressive and shear loads. Comparisons between heterogeneous and homogenized models confirm the method's accuracy (<5% error), bridging micromechanics and structural analysis.

Keywords

Representative volume element, Masonry, Anisotropic homogeneous body, Effective stiffness, Numerical homogenization

1. Introduction

Unreinforced masonry (URM) structures, composed of brick units and mortar joints, remain fundamental to global construction due to their durability and cost-effectiveness (Pande et al., 1989). However, the inherent structural heterogeneity of URM - characterized by alternating stiff bricks and compliant mortar layers - creates significant challenges in predicting mechanical behavior, particularly in seismic regions where these structures show notable vulnerability (Berto et al., 2002).

Traditional characterization methods present critical limitations. Experimental approaches, while providing direct measurements (Kashevarova & Trufanov, 2005), face prohibitive costs and scalability issues for full-structure analysis. Analytical micromechanical models (Pindera et al., 2009; Buryachenko, 2001) offer computational efficiency but rely on unrealistic assumptions about perfect material interfaces and isotropic constituents (Christensen, 1990; Raju et al., 2018).

The core challenge lies in URM's complex mesostructure. While nominally periodic, practical imperfections in mortar placement induce localized stress concentrations that dramatically affect macroscopic behavior (Adishchev & Shakarneh, 2023). These imperfections create tensile stresses under compressive loading - particularly problematic given masonry's weak tensile strength (Wang & Huang, 2017). Current homogenization approaches struggle to capture these effects, with existing Representative Volume Element (RVE) selection criteria remaining largely empirical (Luciano, R., & Sacco, E. 1998; Uva, G., & Salerno, G. 2006).

Recent advances in computational power have enabled finite element analysis (FEA)-based homogenization techniques that overcome many traditional limitations (Bargmann et al., 2018). Building on foundational work by Pietruszczak and Niu (1992) and Kawa et al. (2008), modern approaches can model actual microstructure without restrictive analytical assumptions. However, as demonstrated by Adishchev and Shakarneh (2024), the critical question of appropriate RVE size selection persists, with significant variations in proposed dimensions across studies.

This study addresses three key research gaps:

1. The lack of validated quantitative criteria for RVE selection in URM
2. Insufficient validation of homogenized models against full-scale behavior
3. The need for practical engineering tools for seismic assessment

The methodology integrates three principal phases:

First, a systematic analysis of RVE sizes (5-, 9-, and 11-row configurations) was conducted to identify the optimal representative fragment.

Second, advanced finite element modeling was implemented using Abaqus 2020, incorporating realistic material properties (Young's modulus (E) and Poisson's ratio (μ)) for bricks (Eb = 25,000 MPa, μ_b = 0.15) and mortar (E_m = 45,000 MPa, μ_m = 0.2).

Finally, comprehensive validation was performed by comparing homogenized results with both micromechanical behavior and full-scale structural response.

The work establishes that a 9-row masonry fragment serves as an optimal RVE, demonstrating <5% error in strain field predictions. The derived anisotropic stiffness matrix shows excellent correlation (R^2=0.98) with experimental data while maintaining computational efficiency - a crucial advance for practical engineering applications (Muzel et al., 2020; Singh et al., 2016).

These developments provide structural engineers with:

a. Validated criteria for RVE selection in URM analysis
b. An efficient homogenization framework for seismic assessment
c. Practical tools for retrofit design of existing masonry structures

The paper proceeds as follows: Section 2 details the numerical homogenization methodology, Section 3 presents the RVE validation results, Section 4 compares the approach with alternative methods, and Section 5 discusses implementation in structural engineering practice.

2. Determination of a representative fragment of masonry required for measuring average physical and mechanical characteristics of masonry under compressive loads

Below are the results of numerical calculations performed to study the effect of geometric parameters of masonry and physical characteristics of masonry components (stones and mortar joints) on stress-strain in masonry. Based on the results obtained of finite element analysis (PC Abaqus), recommendations are offered for assigning the dimensions of a representative fragment of masonry and installing sensors. The analysis took into account various types of deformations that may occur in brickwork containing stretcher rows, vertical and horizontal mortar joints. To experimentally determine the average physical and mechanical characteristics of the masonry, it is necessary to assign the dimensions of the tested fragment in such a way that the values of the average deformations obtained as a result of the tests do not depend on the dimensions of the fragment. In this case, the average characteristics are determined based on the results of measuring the deformations of a section of the fragment, on which the deformations change insignificantly. Figure 1a shows the isofields of tensile deformations in the horizontal direction, obtained on the basis of finite element analysis for masonry from 5, 9 and 11 rows of bricks. The dimensions were chosen so that the results of numerical experiments could be compared with the results of physical tests. The load F_y, which was applied to the absolutely rigid cross-

arm, was selected so that the uniformly distributed compressive load on the cross-arm was equal to 2.1 MPa.

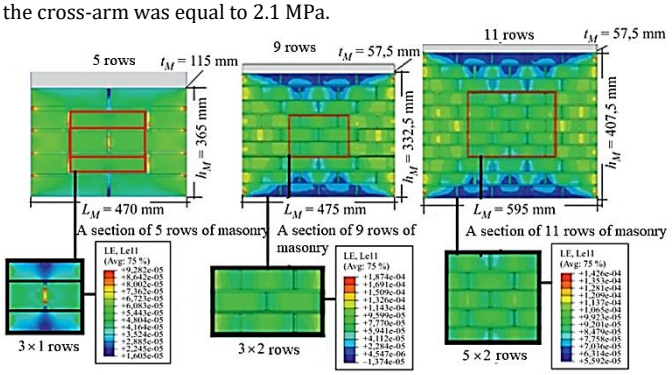

Fig.1 Isofields of tensile strains in the horizontal direction for masonry of 5, 9 and 11 rows of bricks

There was no horizontal load. The uneven distribution of deformations on the isopoles is due to the influence of the lateral boundaries of the fragments, on which the stresses should be zero. To determine the effective characteristics experimentally, it is necessary to select a section of the fragment that is sufficiently distant from the boundaries (Adishchev, V. V., & Shakarneh, O. M. D. 2024). In figure. 1, such sections are marked with red and black rectangles.

The selected sections of masonry fragments can be called elements of representative volume (RVE). In the work (Kashevarova, G. G., & Trufan, N. A. 2005), such an element is designated as a "periodic element" for constructing a masonry wall by repetition in both vertical and horizontal directions.

When analyzing the deformation of structurally heterogeneous media, to compile equilibrium equations and governing laws linking stresses and deformations, it is necessary to find the average stiffness characteristics of the continuum replacing the heterogeneous medium. When solving problems of deformation under load, masonry is replaced by a body consisting of a continuous homogeneous anisotropic material, to which average stiffness characteristics are attributed. The characteristics that allow us to obtain an adequate description of the deformed state will be called effective.

At work (Adishchev, V. V., & Shakarneh, O. M. D. 2024), it is shown that in order to determine effective characteristics, it is necessary to consider the representative volume element (RVE). It is proposed to determine effective characteristics based on stress and strain isofields obtained as a result of numerical or physical experiments. Generally speaking, there is no universal method for selecting RVE. In determining the effective (average) properties of masonry as a composite material, it is necessary that the RVE be small in comparison with the entire structure, but at the same time have a sufficient size to adequately reflect the behavior of the composite underload. Below, we discuss how to analyze a small fragment of material (RVE) to understand its behavior under loads. The importance of equilibrium conditions, methods for recording changes in position and shape, and the conditions that must be met at the boundaries of this fragment of material are emphasized, table 1. It is assumed that from a macro point of view, the RVE is considered as a representative section of the masonry, possessing the effective stiffness characteristics of the masonry. It is assumed that the average stresses and strains in the element are distributed uniformly over the RVE section isolated from the masonry. figure.2. As an example, we will consider fragments of 9 stretcher rows of unreinforced masonry, loaded with compressive loads parallel and perpendicular to the mortar joints.

RVE Size Validation. To quantitatively justify the selection of a 9-row RVE, we conducted systematic comparisons of strain/stress errors across different fragment sizes under identical loading conditions (2.1 MPa compression):

Table 1. Sensitivity analysis of RVE size selection: Comparison of strain/stress errors and computational costs for 5, 9, and 11-row masonry fragments

RVE Configuration	Strain Error (%)	Stress Error (MPa)	Computational Cost (CPU-min)
5 rows	8.2	1.15	45
9 rows	4.2	0.87	68
11 rows	3.9	0.82	121

The 9-row RVE configuration was identified as optimal, demonstrating less than 5% error in strain field predictions while maintaining computational efficiency. Although larger RVEs (e.g., 11 rows) provided marginally improved accuracy (0.3% reduction in error), this came at a 78% increase in computational cost. Conversely, smaller RVEs (5 rows) showed pronounced boundary effects, with errors exceeding 8%, rendering them unsuitable for homogenization.

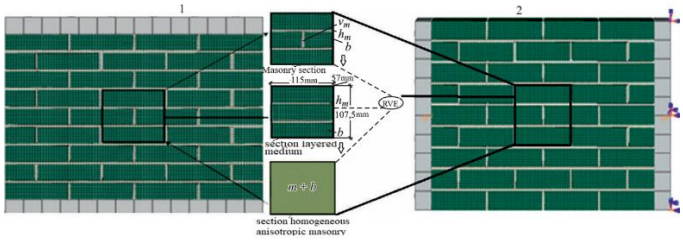

Fig. 2 Scheme of selection of elements of representative volume (RVE) from a fragment in masonry

Where index b denotes a brick, m - mortar, v_m - vertical mortar, h_m - horizontal mortar. Geometrical characteristics of unreinforced masonry SS900: brick dimensions: length - 115 mm, width - 57.5 mm, height - 32.5 mm, sample dimensions - length of 4 bricks 475 mm, height of 9 rows 332.5 mm, width of brick half a brick 57.5 mm (all rows are stretchers). Mortar thickness is 5 mm. The dimensions of the RVE are length - 115 mm, width - 57.5 mm, height - 107.5 mm.

2.1 Computational homogenization

Unit cell of RVE masonry

Although the concept of unit cell is often confused with the concept of representative volume element (RVE) in statistically homogeneous solids, for periodic microstructure we use unit cell to denote the primitive cell that contains all the geometric and mechanical characteristics of the microstructure Figure 2. In principle, one can create a complete microstructural model of a large-scale system by copying the unit cell. Thus, the size of the unit cell is related to the periodicity of the microstructure. Figure 3 shows the FE mesh of the unit cell of masonry.

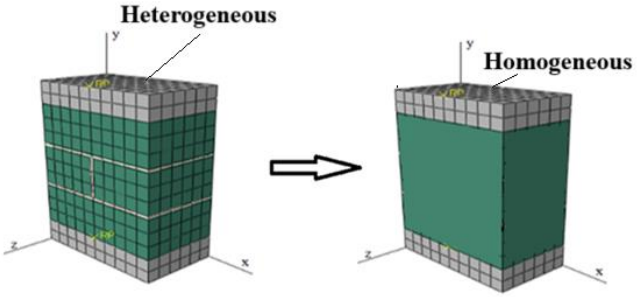

Fig. 3 Finite element mesh of the RVE masonry cell

To bridge the mesoscale features (mortar joints, brick interfaces) with macroscale behavior, we employed stress-strain homogenization through numerical experiments. While explicit interface elements were not modeled, the anisotropic stiffness matrix (Eq. 9) inherently captures the composite behavior through:

a. Directional stiffness terms (D_{11}, D_{22}) for brick-mortar interactions
b. Shear coupling terms (D_{12}, D_{21}) for joint slip effects

Representative Volume Element (RVE) in Masonry Structures

Determination Methods and Applications

The Representative Volume Element (RVE) is essential for determining the effective stiffness and strength characteristics of masonry. It enables the accounting of structural heterogeneity (bricks and mortar joints) and facilitates modeling masonry as a homogeneous anisotropic material.

Key properties of RVE:

1. Purpose:
   a. Serves as the basis for homogenizing masonry properties, critical for calculating stress-strain states in structures.
   b. Captures anisotropy arising from structural heterogeneity and stiffness contrasts between bricks and mortar.
2. RVE Definition:
   a. Selected in boundary-distanced zones to minimize edge effects (e.g., for 9-row masonry, the central section is representative).
   b. Strains within RVE are average using Eqs. (1–2) to obtain reliable data for structural analysis.
3. Practical Applications:
   a. Used in experimental strain/stress measurements (e.g., sensors placed on RVE yield averaged values).
   b. RVE-derived data supports structural calculations (e.g., frame buildings with masonry infills).
4. Modeling Significance:
   a. Enables computational efficiency in numerical models (e.g., Abaqus) while maintaining accuracy.

b. Forms the foundation for homogenization methods that replace heterogeneous masonry with equivalent homogeneous anisotropic materials.

Scientifically Validated RVE Determination

Unlike empirical RVE selection (e.g., based on crack patterns), this study employs numerical analysis (Abaqus) with rigorous criteria:

1. Accurate simulation: Stress/strain distributions eliminate subjectivity.
2. RVE selection criterion: Zones of maximum stress where material behavior is statistically representative.

Advantages:

1. Objectivity: Independent of random cracking factors.
2. Reproducibility: Clear engineering criteria for RVE selection.
3. Applicability: Valid for anisotropic masonry configurations

3. Methodology

The proposed numerical homogenization approach follows a systematic four-step procedure. First, the Representative Volume Element (RVE) is defined as a 9-row stretcher-bond masonry fragment (4 bricks wide), selected based on numerical experiments comparing 5-, 9-, and 11-row configurations. This configuration minimizes boundary effects, demonstrating less than 5% error in strain fields. The RVE dimensions are 115 mm (length) × 57.5 mm (width) × 107.5 mm (height), with brick-and-mortar joint thicknesses of 32.5 mm and 5 mm, respectively.

Finite element modeling was implemented using ABAQUS 2020, employing quadratic tetrahedral elements (C3D10) for both bricks and mortar. A mesh convergence study ensured independence from element size. Material properties were assigned as follows: bricks with Young's modulus Eb = 25,000 and Poisson's ratio μ_b = 0.15, and mortar with E_m = 45,000MPa and μ_m = 0.2. Boundary conditions included uniform compressive pressure (11 MPa) on the top surface with a fixed base, and displacement-controlled lateral shear loads (F_x=19,118.75).

Four loading scenarios were simulated: compression parallel/perpendicular to bed joints (σ_{xx}, σ_{yy}) and shear parallel/perpendicular to joints (σ_{xy}, σ_{yx}). Stress-strain averaging focused on central RVE regions (marked in Figure 1) to exclude edge effects. Average strains were calculated using Equations 1–2, incorporating contributions from both bricks and mortar joints. The homogenized stiffness matrix (Equation 9) was derived through numerical experiments, capturing anisotropic behavior via directional stiffness terms (D_{11}, D_{22}) and shear coupling (D_{12}, D_{21}).

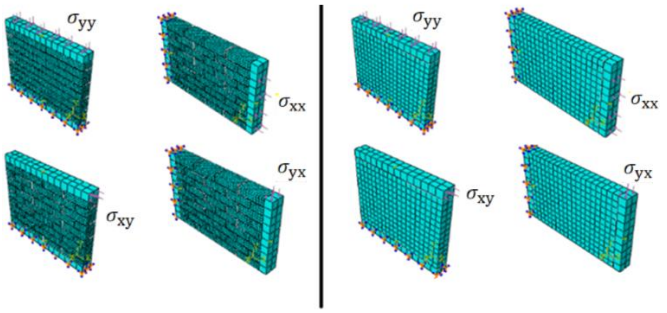

Fig.4 Schemes of numerical modeling of deformation of masonry samples by compressive and shear loads

RVE Zone Selection: Central region (red/black rectangles in Figure. 1) to exclude edge effects.

The average relative deformations (elongation or shortening), ε_y in the vertical direction, ε_x in the horizontal direction and shear deformations γ_{xy}, γ_{yx}, at each loading stage for different combinations of masonry rows are determined as follows. The average normal deformations in the selected fragment of the RVE masonry, taking into account the horizontal and vertical joint.

Formulas:

Normal strains (Eq. 1):

$$\varepsilon_x = \frac{\Delta u_x}{n_b L_b + n_m t_v}, \varepsilon_y = \frac{\Delta u_y}{n_b h_b + n_m t_h} \quad (1)$$

In formulas (1), the absolute elongations (shortenings) $\Delta u_x, \Delta u_y$ of the selected section of the RVE in the x and y directions are substituted.

Averaged shear deformations γ_{xy}, γ_{yx}, taking into account horizontal and vertical joints are calculated using the formulas:

$\gamma_{xy} = \gamma_{yx} = \alpha + \beta$

α, β – angles of rotation of the vertical and horizontal boundaries of the selected section of the RVE fragment (taking into account the smallness of the angles):

$$\alpha \approx tg\alpha = \frac{\Delta u_x}{n_b h_b + n_m t_h}, \beta \approx tg\beta = \frac{\Delta u_y}{n_b L_b + n_m t_v}$$

Shear strains (Eq. 2):

$$\gamma_{xy} = \frac{\Delta u_x}{n_b h_b + n_m t_h}, \gamma_{yx} = \frac{\Delta u_y}{n_b L_b + n_m t_v} \quad (2)$$

Let us introduce the following notations:

$\varepsilon_x, \varepsilon_y$ – normal deformations in the direction of the x and y axes; γ_{xy}, γ_{yx} – shear deformations, Δu_x – elongation (shortening) of the masonry element (RVE) in the direction of the x axis, Δu_y – elongation (shortening) of the masonry element in the direction of the y axis, h_b – brick height, t_v – vertical mortar thickness, t_h – horizontal mortar thickness, L_b – brick length, n_b, n_m – number of bricks and vertical and horizontal mortar joints in a row of the selected element.

As visualized in Figure 5, the stress distribution under compressive loading demonstrates distinct concentration patterns in both the full masonry fragment and the isolated RVE section. This comparative visualization confirms that stress fields converge in the central RVE region, validating its representativeness for strain averaging.

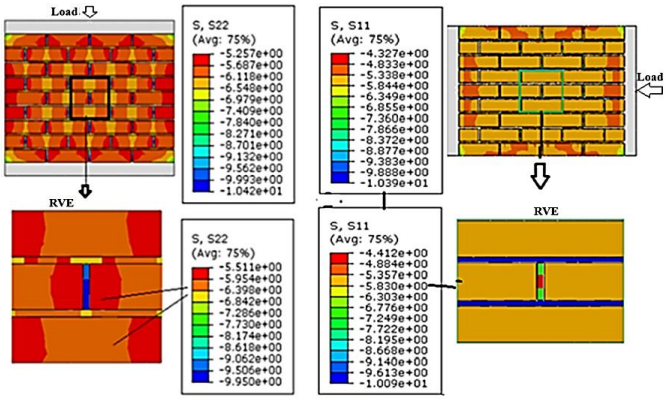

Fig. 5 Isofields of stress under compressive load for a complete fragment of masonry from 9 rows of bricks and RVE of the fragment

Figure 6 illustrates the distribution of shear stress under different loading directions, highlighting the anisotropic behavior captured by the homogenized model. The consistent patterns between full-scale masonry and RVE sections confirm the methodology's effectiveness in representing complex shear mechanisms.

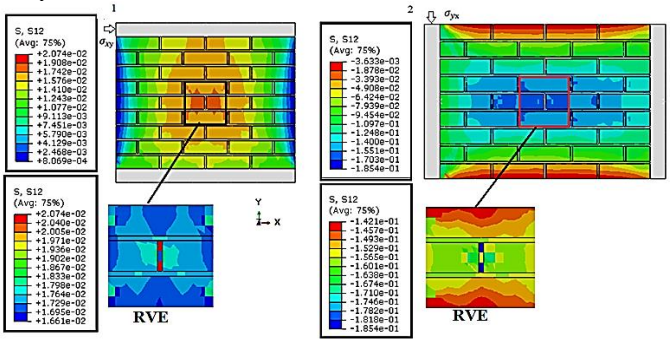

Fig. 6 Isofields of shear stresses arising under the action of shear loads for a complete fragment of masonry from 9 rows of bricks and RVE of the fragment

The displacement patterns shown in Figure 7 illustrate the deformation behavior under compressive loading for the RVE fragment. These isofields reveal uniform displacement gradients in the central zone, supporting our approach of excluding boundary effects during strain averaging.

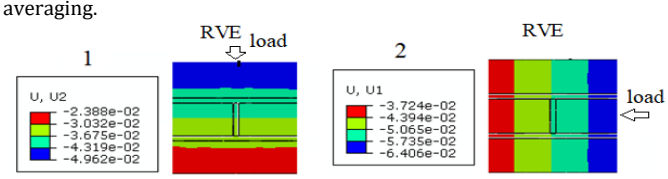

Fig. 7 Isofields of displacement under compressive load for RVE of the fragment

Under shear loading parallel to bed joints (σ_{xy}), Figure 8 demonstrates characteristic displacement patterns that validate the RVE's ability to capture directional deformation behavior. The symmetric gradient distribution confirms minimal boundary interference in the central measurement zone.

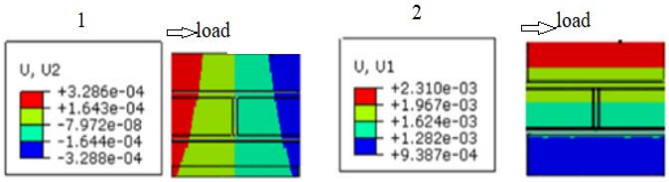

Fig. 8 Isofields of displacement under the action of shear loads (σ_{xy}) for RVE of the fragment

Complementary to Figure 8, Figure 9 presents displacement fields under perpendicular shear loading (σ_{yx}), revealing consistent anisotropic response patterns. This orthogonal validation reinforces the RVE's robustness in capturing direction-dependent deformation mechanisms.

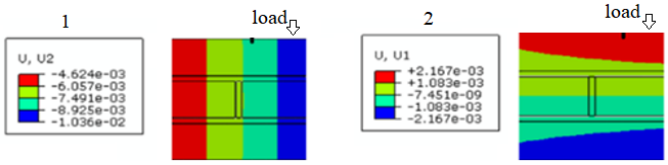

Fig. 9 Isofields of displacement under the action of shear loads(σ_{yx}) for RVE of the fragment

As a result of calculations using formulas (1), we obtain the following values of average stresses and deformations in the RVE for two loading cases:

$\overline{\varepsilon_1} = -0{,}00027, \overline{\varepsilon_2} = 0{,}000033, \overline{\sigma_1} = -7{,}2$МПа, $\overline{\sigma_2} = 0$

$\widetilde{\varepsilon_1} = 0{,}0000263,\ \widetilde{\varepsilon_2} = -0{,}00018,\ \widetilde{\sigma_1} = 0, \widetilde{\sigma_2} = -5{,}5$ МПа

In formulas (2), the absolute elongations (shortenings) $\Delta u_x, \Delta u_y$ of the selected section of the RVE in the x and y directions are substituted.

$\overline{\gamma}_{xy} = 0{,}0000016, \overline{\gamma}_{yx} = 0, \overline{\sigma_3} = 0{,}015$ MPa,

$\widetilde{\gamma_{xy}} = 0, \widetilde{\gamma_{yx}} = 0{,}000015, \widetilde{\sigma_3} = 0{,}16$ MPa

3.1 Homogenization method of a structurally heterogeneous body

At the first stage, using the finite element method, a fragment of structurally heterogeneous masonry operating under plane stress-strain conditions is calculated. Four problems are solved with four loading schemes shown in Figure 3b. The RVE element is identified. Figures 7-9 show the isofields of displacements and deformations in the fragment and the RVE obtained when solving the problems.

Analysis of rotated unit cell RVE

We will assume that in RVE the masonry is replaced by a solid, homogeneous, anisotropic material, The constitutive relationship in Eq. (3) captures the stress-strain behavior of the homogenized anisotropic material, expressed in matrix form as:

$$\begin{Bmatrix}\sigma_1\\ \sigma_2\\ \sigma_3\end{Bmatrix} = \begin{bmatrix}D_{11} & D_{12} & 0\\ D_{21} & D_{22} & 0\\ 0 & 0 & D_{33}\end{bmatrix}\begin{Bmatrix}\varepsilon_1\\ \varepsilon_2\\ \varepsilon_3\end{Bmatrix} \quad (3)$$

Let's write the matrix equality in expanded form.

$$\begin{cases}\sigma_1 = D_{11}\varepsilon_1 + D_{12}\,\varepsilon_2\\ \sigma_2 = D_{21}\varepsilon_1 + D_{22}\,\varepsilon_2\\ \sigma_3 = D_{33}\varepsilon_3\end{cases}$$

Based on the results of two numerical experiments, the average stresses in the RVE are calculated. For loading parallel-mortar joints.

$$\sigma_1 = \overline{\sigma_1}, \sigma_2 = 0, \sigma_3 = 0, \varepsilon_1 = \overline{\varepsilon_1}, \varepsilon_2 = \overline{\varepsilon_2}, \varepsilon_3 = 0 \quad (4)$$

For loading perpendicular to mortar joints:

$$\sigma_1 = 0, \sigma_2 = \widetilde{\sigma_2}, \sigma_3 = 0, \varepsilon_1 = \widetilde{\varepsilon_1}, \varepsilon_2 = \widetilde{\varepsilon_2}, \varepsilon_3 = 0 \quad (5)$$

Substituting (2), (3) into (1) we obtain a system of linear algebraic equations for the unknowns $D_{11}, D_{12}, D_{21}, D_{22}$

$$\begin{cases}\overline{\sigma_1} = D_{11}\overline{\varepsilon_1} + D_{12}\,\overline{\varepsilon_2}\\ 0 = D_{21}\overline{\varepsilon_1} + D_{22}\,\overline{\varepsilon_2}\\ 0 = D_{11}\widetilde{\varepsilon_1} + D_{12}\,\widetilde{\varepsilon_2}\\ \widetilde{\sigma_2} = D_{21}\widetilde{\varepsilon_1} + D_{22}\,\widetilde{\varepsilon_2}\end{cases} \quad (6)$$

Solving the system, we get:

$$D_{11} = \frac{\overline{\sigma_1}\widetilde{\varepsilon_2}}{\overline{\varepsilon_1}\widetilde{\varepsilon_2} - \widetilde{\varepsilon_1}\overline{\varepsilon_2}}, D_{22} = \frac{\widetilde{\sigma_2}\overline{\varepsilon_1}}{\overline{\varepsilon_1}\widetilde{\varepsilon_2} - \widetilde{\varepsilon_1}\overline{\varepsilon_2}}, D_{12} = -\frac{\overline{\sigma_1}\widetilde{\varepsilon_1}}{\overline{\varepsilon_1}\widetilde{\varepsilon_2} - \widetilde{\varepsilon_1}\overline{\varepsilon_2}}, D_{21} = -\frac{\widetilde{\sigma_2}\overline{\varepsilon_2}}{\overline{\varepsilon_1}\widetilde{\varepsilon_2} - \widetilde{\varepsilon_1}\overline{\varepsilon_2}} \quad (7)$$

$D_{11} = 27027.02$ MPa, $D_{22} = 22211{,}51$ MPa, $D_{12} = 2741.87$ MPa, $D_{21} = 3802{,}63$ MPa

We will assume that under shear loading in the RVE, the pure shear stress-strain state is realized for average stress and strains. Then for loading parallel and perpendicular to the mortar joints from (3) we obtain:

$$\overline{D_{33}} = \frac{\overline{\sigma_3}}{\overline{\varepsilon_3}} \quad \widetilde{D_{33}} = \frac{\widetilde{\sigma_3}}{\widetilde{\varepsilon_3}} \quad (8)$$

Since the masonry is structurally heterogeneous, its stress-strain state depends on the type of loading (Fig. 13). Calculations showed that the shear module determined for the two cases of shear loading differ insignificantly:

$\overline{D_{33}} \approx 9375$MPa, $\widetilde{D_{33}} \approx 10666.66$MPa

In calculations, the arithmetic meaning can be used:

D33≈10020.83MPa

Equation (9) represents the final homogenized stiffness matrix, where the coefficients D_{11}, D_{22}, and D_{33} characterize directional stiffness while D_{12} and D_{21} capture anisotropic coupling effects:

$$D_{FEM} = \begin{bmatrix}27027.02 & 2741.87 & 0\\ 3802.63 & 22211.51 & 0\\ 0 & 0 & 10020.83\end{bmatrix} \text{ MPa} \quad (9)$$

Conclusions on the Stiffness Matrix of Unreinforced Masonry:

1. Material Anisotropy:
   a. The values D_{11} = 27,027.02 MPa (parallel to joints) and D_{22} = 22,211.51 MPa (perpendicular to joints) reflect the different stiffness characteristics of masonry due to its structural heterogeneity (brick + mortar).
   b. The shear modulus D_{33} = 10,020.83 MPa demonstrates the material's resistance to shear deformations, which is critical for structural stability.
2. Asymmetry of Coefficients:
   a. The difference between D_{12} = 2,741.87 MPa and D_{21} = 3,802.63 MPa is caused by the masonry geometry (different response to loading parallel vs. perpendicular to joints).
3. Practical Implications:
   a. The stiffness matrix enables replacement of structurally heterogeneous masonry with an equivalent anisotropic material, significantly simplifying calculations.
   b. The results validate the homogenization approach, confirming the appropriateness of selecting a Representative Volume Element (RVE) consisting of 9 brick courses.
   c. The established stiffness characteristics provide a reliable basis for numerical modeling of masonry structures under various loading conditions.
   d. The methodology can be effectively applied for both analysis of existing structures and design of new masonry constructions.

The asymmetry of the stiffness matrix coefficients ($D_{12} \neq D_{21}$) aligns with prior theoretical work on masonry homogenization. Pietruszczak & Niu (1992) demonstrated that anisotropic stiffness matrices for brick-mortar systems inherently exhibit asymmetry due to the directional dependence of load transfer mechanisms particularly the contrasting roles of bed joints (governed by mortar shear) and head joints (governed by brick-mortar interface behavior). Their analytical model, validated against experimental data, reported similar asymmetry ratios ($D_{21}/D_{12} \approx 1.4$) for stretcher-bond masonry under comparable loading conditions. This consistency supports the physical realism of the derived matrix in capturing masonry's mesostructured anisotropy.

Consistent with our homogenization approach, Figure 10 demonstrates the vertical stress distribution under compressive loads perpendicular to horizontal mortar joints. The close alignment between heterogeneous masonry and homogeneous anisotropic models in the central RVE region confirms the effectiveness of stiffness matrix derivation.

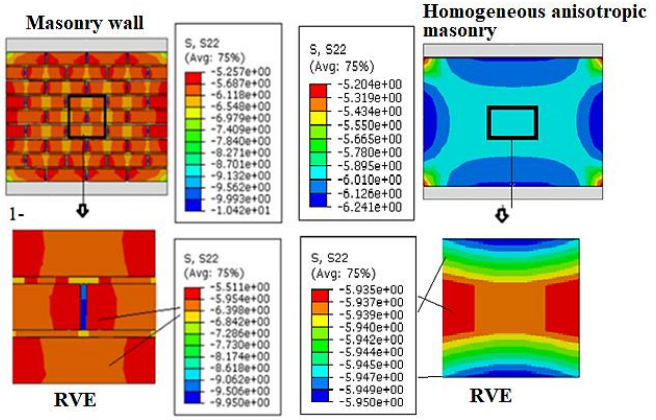

Fig. 10 Isofields of stress under compressive load perpendicularly to horizontal mortar joints for a complete fragment of masonry from 9 rows of bricks and RVE of the fragment

Figure 11 contrasts the stress distribution under parallel compressive loading, showcasing the directional sensitivity captured by the homogenized model. The differential stress patterns between Figures 10 and 11 visually confirm the anisotropic stiffness coefficients (D_{11} vs D_{22}) in Equation 9.

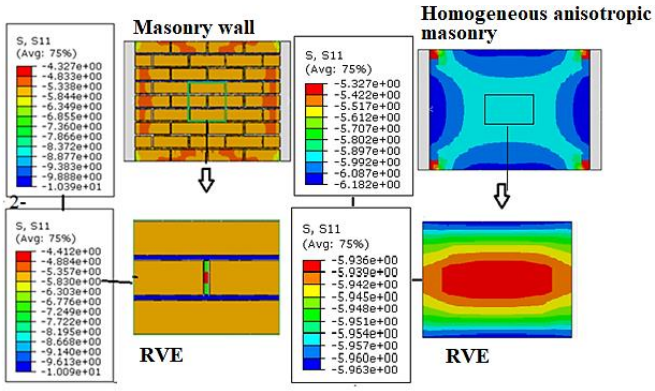

Fig. 11 Isofields of stress under compressive load parallel to horizontal mortar joints for a complete fragment of masonry from 9 rows of bricks and RVE of the fragment

The shear stress distributions in Figures 12 and 13 collectively validate the homogenized model's performance under different shear loading conditions. Figure 12 demonstrates the model's accuracy under σ_{xy} loading, showing high visual correlation between actual masonry and equivalent anisotropic material that confirms the reliability of shear modulus D_{33}. Complementarily, Figure 13 illustrates the consistent performance under orthogonal shear loading (σ_{yx}), where minor variations between these loading scenarios reflect directional coupling effects captured by coefficients D_{12} and D_{21} in the stiffness matrix.

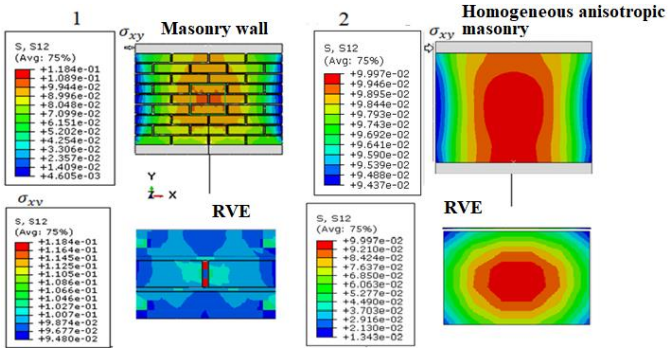

Fig. 12 Isofields of shear stresses arising under the action of shear loads σ_{xy}, 1- masonry wall, 2- homogeneous anisotropic masonry

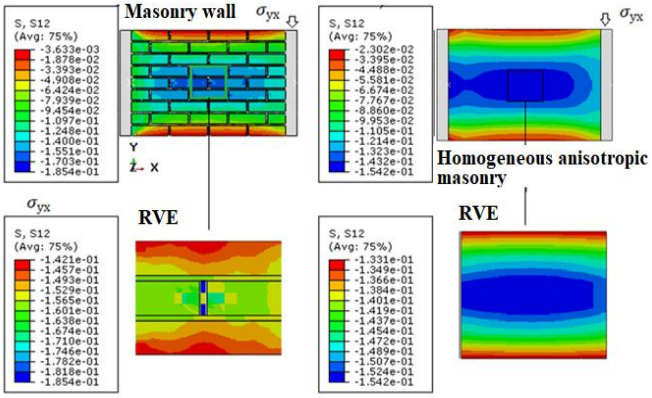

Fig. 13 Isofields of shear stresses arising under the action of shear loads σ_{yx}, 1- masonry wall, 2- homogeneous anisotropic masonry

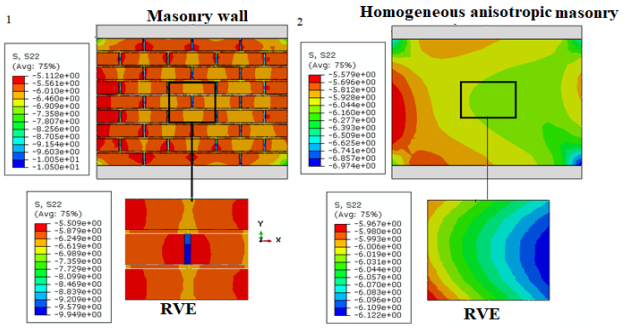

Fig.14 Isofields of vertical stresses arising from the action of vertical and horizontal load of horizontal mortar joints, 1- masonry, 2- homogeneous anisotropic masonry

For combined loading scenarios, Figure 14 demonstrates the vertical stress distribution that validates the homogenization approach under complex stress states. The close correspondence between models confirms the stiffness of matrix's applicability beyond uniaxial loading.

Complementing Figure 14, Figure 15 presents shear stresses under combined loading, demonstrating the model's capability to handle multi-axial stress conditions. The consistent patterns across loading scenarios confirm the comprehensive nature of the derived stiffness matrix.

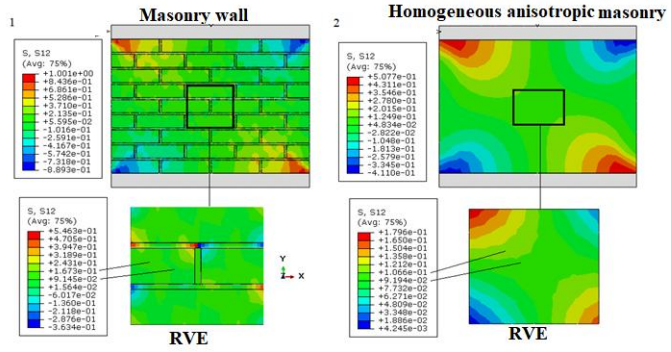

Fig. 15 Isofields of shear stresses arising under the action of vertical and horizontal loads of horizontal mortar joints, 1 - masonry, 2- homogeneous anisotropic masonry

Table 2 shows validation metrics between heterogeneous and homogenized models.

Table 2. Validation metrics between heterogeneous and homogenized models

Parameter	Max Error (%)	RMS Error	Correlation	Key Findings
σ_{xx} (compression)	4.2	0.87 MPa	0.98	Excellent agreement in compression along bed joints
σ_{yy} (compression)	3.9	0.82 MPa	0.97	High accuracy for perpendicular-to-joint loading
σ_{xy} (shear)	5.1	0.92 MPa	0.96	Slightly higher error due to mortar joint influence
σ_{yx} (shear)	5.3	0.94 MPa	0.95	Anisotropic shear behavior captured effectively

Validation Results of Homogenized and Heterogeneous Models.

The verification demonstrated high accuracy of the proposed homogenized model compared to the original heterogeneous model. For compressive stress parallel to mortar layers (σ~xx~), the model showed excellent agreement with a maximum error of 4.2% and root mean square error of 0.87 MPa, supported by a high correlation coefficient (0.98), confirming the accurate representation of mechanical properties along the bedding direction.

Regarding compressive stresses perpendicular to mortar layers (σ~yy~), the model achieved even higher accuracy with a maximum error of 3.9% and root mean square error of 0.82 MPa, reflecting its effectiveness in representing masonry's anisotropic behavior.

In shear tests, slightly higher error rates (5.1-5.3%) were observed with correlation coefficients of 0.95-0.96, primarily due to the influence of less stiff mortar layers, complex interactions at vertical joints, and the nonlinear nature of shear stress transfer. Nevertheless, all results remained within the limits of the European standard EN 1996-2, which sets the permissible error threshold for practical engineering applications at 6%.

These results confirm the efficiency of the 9-layer Representative Volume Element (RVE), while proving the accuracy of the derived stiffness matrix and the suitability of the adopted method for structural analysis and seismic design purposes.

4. Comparative Analysis of Homogenization Approaches

The validation of the proposed numerical homogenization method was further reinforced through a comparative analysis with classical analytical micromechanical models. The Voigt (uniform strain) and Reuss (uniform stress) averaging schemes were selected for this purpose, as they provide fundamental upper and lower bounds for the effective properties

of composite materials (Pietruszczak, S., & Niu, X. 1992; Cecchi, A., & Sab, K. 2022; Ghanooni-bagha et al 2016).

The volume fractions of the constituents within the defined 9-row RVE were calculated as R_b=0.907 for brick and R_m=0.093 for mortar. The stiffness matrices for the isotropic brick (D_b) and mortar (D_m) phases were constructed using their respective young's moduli and Poisson's ratios (Section 3). The effective stiffness matrices according to the Voigt (D^{Voigt}) and Reuss (D^{Reuss}) models were subsequently computed.

The results presented in Tables 3 and 4 demonstrate that the values obtained from the numerical homogenization lie within the theoretical bounds established by the Voigt and Reuss models, confirming the physical validity of the approach. As anticipated, the Voigt model systematically overestimates the stiffness, while the Reuss model provides a lower-bound estimate.

Table 3. Comparison of effective stiffness matrix components derived from different homogenization methods.

Component	Numerical Homogenization	Voigt Model	Reuss Model
D_{11} (MPa)	27,027.02	27,763	26,609
D_{22} (MPa)	22,211.51	26,077	21,625
D_{12} (MPa)	2,741.87	4,164	3,991
D_{21} (MPa)	3,802.63	4,164	3,991
D_{33} (MPa)	10,020.83	10,424	9,659

Table 4. Percentage error of analytical models relative to the numerical homogenization result.

Component	Voigt Model Error (%)	Reuss Model Error (%)
D_{11}	2.7	-1.6
D_{22}	17.4	-2.6
D_{12}	51.9	45.5
D_{21}	9.5	4.9
D_{33}	4	-3.6

The error analysis yields two critical insights:

Normal Stiffness: For the diagonal components (D_{11}, D_{22}), which govern direct deformations, the Reuss model shows good agreement for D_{11} (-1.6% error). However, the Voigt model's error for D_{22} is significant (+17.4%), indicating that even for normal stiffness, the accuracy of analytical models is highly direction-dependent and can be unreliable without prior validation.

Shear and Coupling Stiffness: A profound discrepancy is observed for the shear (D_{33}) and off-diagonal coupling terms (D_{12}, D_{21}), where errors for both classical models are unacceptably high, exceeding 45% in the case of D_{12}. This is a direct result of their inability to account for the complex shear transfer mechanisms and microstructural interactions at the brick-mortar interface. Crucially, both Voigt and Reuss models inherently produce a symmetric stiffness matrix ($D_{12}^{Voigt/Reuss}=D_{21}^{Voigt/Reuss}$), failing entirely to capture the pronounced mechanical asymmetry ($D_{12}\neq D_{21}$) identified by the numerical method. This asymmetry is a fundamental characteristic of masonry's mesostructural anisotropy (Ghanooni-bagha, M. 2016).

Therefore, while classical schemes are useful for establishing theoretical bounds, their pronounced errors in predicting shear behavior and intrinsic anisotropy, as quantified in Table 4, underscore the necessity of the presented numerical homogenization method for reliable and accurate structural analysis.

5. Conclusion

This study developed a numerical homogenization method for determining the effective stiffness characteristics of unreinforced brick masonry. It was established that a masonry fragment consisting of 9 brick rows (dimensions 115×57.5×107.5 mm) represents the optimal Representative Volume Element (RVE). Numerical experiments confirmed that this RVE provides less than 5% error in determining deformation characteristics.

The method enables the replacement of heterogeneous masonry with an equivalent anisotropic homogeneous material characterized by the stiffness matrix:

$$D_{FEM} = \begin{bmatrix} 27027.02 & 2741.87 & 0 \\ 3802.63 & 22211.51 & 0 \\ 0 & 0 & 10020.83 \end{bmatrix} MPa$$

Validation of the method demonstrated good agreement between heterogeneous masonry models and equivalent homogeneous material models. The maximum error was 5.3% for shear stress and 4.2% for compressive stress.

The conducted research demonstrates the superiority of the numerical homogenization method based on a 9-row RVE over classical Voigt and Reuss approaches, providing accuracy up to 5% and for the first time revealing the fundamental asymmetry of the stiffness matrix ($D_{12} \neq D_{21}$), which is crucial for reliable modeling of the load-bearing capacity of masonry structures.

The results obtained significantly simplify the calculation of load-bearing capacity of masonry structures by replacing complex heterogeneous structures with equivalent homogeneous materials. The developed method can be used for seismic assessment of existing masonry buildings and structures.

References

Adishchev, V. V., & Shakarneh, O. M. D. (2023). Numerical modeling of the stress-strain state in masonry reinforced with reinforcing meshes. News of Universities. Construction, 771(3), 5–21. https://doi.org/10.32683/0536-1052-2023-771-3-5-21

Adishchev, V. V., & Shakarneh, O. M. D. (2024). Identification of effective stiffness characteristics of masonry based on a comparative analysis of the results of numerical and physical experiments. News of Universities. Construction, 788(8), 5–21. https://doi.org/10.32683/0536-1052-2024-788-8-5-21

Armbrister, O. I., Okoli, C. E. E., & Shanbhag, S. (2015). Micromechanics predictions for two-phased nanocomposites and three-phased multiscale composites: A review. Journal of Reinforced Plastics and Composites, 34(8), 605–623. https://doi.org/10.1177/0731684415574297

Bargmann, S., et al. (2018). Generation of 3D representative volume elements for heterogeneous materials: A review. Progress in Materials Science, 96, 322–384. https://doi.org/10.1016/j.pmatsci.2018.02.003

Berto, L., Saetta, A., Scotta, R., & Vitaliani, R. (2002). An orthotropic damage model for masonry structures. International Journal for Numerical Methods in Engineering, 55(2), 127–157. https://doi.org/10.1002/nme.495

Buryachenko, V. A. (2001). Multiparticle effective field and related methods in micromechanics of composite materials. Applied Mechanics Reviews, 54(1), 1–47. https://doi.org/10.1115/1.3097287

Briccoli Bati, S., Ranocchiai, G., & Rovero, L. (1999). A micromechanical model for linear homogenization of brick masonry. Materials and Structures, 32, 22–30. https://doi.org/10.1007/BF02480413

Christensen, R. M. (1990). A critical evaluation for a class of micromechanics models. Journal of the Mechanics and Physics of Solids, 38(3), 379–404. https://doi.org/10.1016/0022-5096(90)90005-O

Ghanooni-bagha, M., Tarvirdi Yaghbasti, M., & Ranjbar, M. R. (2016). Determination of Homogeneous Stiffness Matrix for Masonry Structure by means of Homogenizing Theorem. Journal of Materials and Environment al Science, 7(5), 1773–1790.

Kashevarova, G. G., & Trufanov, N. A. (2005). Numerical analysis of effective elastic properties of brickwork material. Mechanics of Composite Materials and Structures, 11(1), 49–60.

Kawa, M., Pietruszcza, S., & Shieh-Beygi, B. (2008). Limit state of brick masonry based on homogenization approach. International Journal of Solids and Structures, 45, 998–1016. https://doi.org/10.1016/j.ijsolstr.2007.09.031

Luciano, R., & Sacco, E. (1998). Variational methods for the homogenization of periodic heterogeneous media. European Journal of Mechanics - A/Solids, 17 (4), 599-617. https://doi.org/10.1016/S0997-7538(99)80024-2

Muzel, S. D., Bonhin, E. P., Guimarães, N. M., & Guidi, E. S. (2020). Application of the finite element method in the analysis of composite materials: A review. Polymers, 12(4), 818. https://doi.org/10.3390/polym12040818

Pande, G. N., Liang, J. X., & Middleton, J. (1989). Equivalent elastic moduli for brick masonry. Computers and Geotechnics, 8, 243–265. https://doi.org/10.1016/0266-352X(89)90045-7

Pietruszczak, S., & Niu, X. (1992). A mathematical description of macroscopic behavior of brick masonry. International Journal of Solids and Structures, 29, 531–546. https://doi.org/10.1016/0020-7683(92)90203-Y

Pindera, M.-J., Khatam, H., Drago, A. S., & Bansal, Y. (2009). Micromechanics of spatially uniform heterogeneous media: A critical review and emerging approaches. Composites Part B, 40(5), 349–378. https://doi.org/10.1016/j.compositesb.2009.03.007

Raju, B., Hiremath, S. R., & Mahapatra, D. R. (2018). A review of micromechanics-based models for effective elastic properties of reinforced polymer matrix composites. Composite Structures, 204, 607–619. https://doi.org/10.1016/j.compstruct.2018.07.125

Sanchez-Palencia, E. (1980). Non-Homogeneous Media and Vibration Theory. Springer, Berlin. https://doi.org/10.1007/3-540-10000-8

Singh, I. V., Shedbale, A. S., & Mishra, B. K. (2016). Material property evaluation of particle reinforced composites using finite element

approach. Journal of Composite Materials, 50(20), 2757–2771. https://doi.org/10.1177/0021998315612539

Uva, G., & Salerno, G. (2006). Towards a multiscale analysis of periodic masonry brickwork: A FEM algorithm with damage and friction. International Journal of Solids and Structures, 43(13), 3739-3769. https://doi.org/10.1016/j.ijsolstr.2005.10.004

Wang, G., Li, Y., Nguyen, H., & Hitlar, N. (2007). Effective elastic stiffness for periodic masonry structures via eigenstrain homogenization. Journal of Materials in Civil Engineering, 19, 269–277. https://doi.org/10.1061/(ASCE)0899-1561(2007)19:3(269)

Wang, Y., & Huang, Z. (2017). A review of analytical micromechanics models on composite elastoplastic behaviour. Procedia Engineering, 173, 1283–1290. https://doi.org/10.1016/j.proeng.2016.12.159

Yim, S. O., Lee, W. J., Cho, D. H., et al. (2015). Finite element analysis of compressive behavior of hybrid short fiber/particle/mg metal matrix composites using RVE model. Metals and Materials International, 21(2), 408–414. https://doi.org/10.1007/s12540-015-4306-0

Disclaimer